ÖAW AUSTRIAN ACADEMY OF SCIENCES

RICAM – JOHANN RADON INSTITUTE FOR COMPUTATIONAL AND APPLIED MATHEMATICS

The algebraic range of the planar X-ray transform of symmetric tensors and applications to noise reduction

H. Fujiwara, K. Sadiq, A. Tamasan

RICAM-Report 2023-09

The algebraic range of the planar X-ray transform of symmetric tensors and applications to noise reduction

Hiroshi Fujiwara[1], Kamran Sadiq[2] and Alexandru Tamasan[3]

[1] Graduate School of Informatics, Kyoto University, Yoshida Honmachi, Sakyo-ku, Kyoto 606-8501, Japan
fujiwara@acs.i.kyoto-u.ac.jp

[2] Johann Radon Institute for Computational and Applied Mathematics (RICAM), Altenbergerstrasse 69, 4040 Linz, Austria
kamran.sadiq@ricam.oeaw.ac.at

[3] Department of Mathematics, University of Central Florida, Orlando, 32816 Florida, USA
tamasan@math.ucf.edu

Abstract. We define the algebraic range $AR(X)$ of the X-ray transform of symmetric tensors via the algebraic constraints of the Fourier coefficients on the lattice $\mathbb{Z} \times \mathbb{Z}$, recently introduced by the authors. The algebraic range is the L^2-closure of the range of the X-ray transform of smooth tensors of compact support. Orthogonal projection of the data on $AR(X)$ reduces the noise by annihilating its orthogonal component. In numerical experiments for 0-order tensors we illustrate the effect of inverting the X-ray transform from such projections.

Keywords: X-ray transform, Radon transform, fan-beam coordinates, symmetric tensors, generalized Gelfand-Graev-Helgason-Ludwig moment conditions, noise reduction

1 Introduction

This work concerns the X-ray transform of symmetric real valued tensors $\mathbf{f}$ with square integrable components supported in the unit disc. The X-ray transform of $\mathbf{f}$ in the fan-beam coordinates is extended by anti-symmetry to a square integrable function $(e^{\mathrm{i}\beta}, e^{\mathrm{i}\theta}) \mapsto \sum_{n=-\infty}^{\infty} \sum_{k=-\infty}^{\infty} g_{n,k} e^{\mathrm{i}n\theta} e^{\mathrm{i}k\beta}$ on the entire torus.

In [16, 17] the authors use tools from the A-analytic theory [1, 15] and characterize the range of the X-ray transform in terms of the Fourier coefficients $\{g_{n,k}\}$. In here we give an alternate derivation of the necessary constraints without appeal to A-analyticity. As a fringe, the new proof connects the characterization in [17] with the one in [12], which, in turn, generalizes the classical characterization in [3, 5, 9] for (rapidly decaying) 0-tensors; for brevity we call the latter the Gelfand-Graev, Helgason, and Ludwig (GGHL)-characterization. A quite different characterization in [14] was given for symmetric tensors of order 0 and 1 on simple Riemannian surfaces with boundary. The connection between the GGHL-characterization and the Euclidean version of the characterization result in [14] was established in [10].

Use of the constraints in the range of the X-ray transform has been known to correct for motion artifacts [20, 21], completion of data [19, 4, 7, 8], or CT-hardware failure diagnosis [13]. In the space of square integrable functions on the torus, our new characterization in [17] naturally define the *algebraic range* $AR(X)$, which we show to be the closure (in L^2) of the range of the X-ray transform of smooth tensors of compact support. Orthogonal projection of the data on the algebraic range reduces the noise, by annihilating its component orthogonal to $AR(X)$. We use the projection method in numerical experiments with 0-order tensors, and illustrate the effect it renders in the reconstruction.

In Section 2 we establish notation and recall the necessity part of the characterization in [17]. In Section 3 we present an alternate proof of the necessary constraints in the X-ray data. In Section 4 we introduce the *algebraic range* and its approximation by some specific band limited subspaces. In numerical experiments in Section 5 we illustrate the effect produced by our denoising by projection method to the reconstruction.

While the change of parity in the order of the tensor propagates to every level of the proofs, it produces merely nominal changes. For the sake of clarity we present here only the even order case, which includes the application in X-ray tomography.

While this work concerns problems in two dimensions, it should be mentioned that in three dimensions, the characterization is of a different nature, where the X-ray transform satisfy John equation [6] for 0-order tensor, and later extended to higher order tensors in [11].

2 Preliminaries

Let $\mathbf{f} = (f_{i_1 i_2 \dots i_m})$, with $i_1, ..., i_m \in \{1, 2\}$ be a real valued symmetric m-tensor, with components of compact support in the plane. By scaling and translating, we may assume that all its components are supported inside the unit disc Ω,

$$\text{supp } f_{i_1 \dots i_m} \subset \Omega. \tag{2.1}$$

When the components of $\mathbf{f}$ are also in $L^p(\Omega)$, we adapt the notation in [18]:

$$L^p_0(\mathbf{S}^m; \Omega) = \{\mathbf{f} = (f_{i_1 \cdots i_m}) \in \mathbf{S}^m(\Omega) : f_{i_1 \cdots i_m} \in L^p(\Omega), \text{ satisfying (2.1)}\}.$$

The boundary of the domain is the unit circle Γ, but we keep this notation to differentiate from the set $\mathbb{S}^1$ of directions. The symmetry refers to the components $f_{i_1 i_2 \dots i_m}$ being invariant under any transposition of indexes. For $\boldsymbol{\theta} = \langle \theta^1, \theta^2 \rangle = \langle \cos\theta, \sin\theta \rangle$, let $\boldsymbol{\theta}^m := \underbrace{\boldsymbol{\theta} \otimes \boldsymbol{\theta} \otimes \cdots \otimes \boldsymbol{\theta}}_{m} \in \left(\mathbb{S}^1\right)^m$. For any $x \in \Omega$, let

$$\langle \mathbf{f}(x), \boldsymbol{\theta}^m \rangle = \sum_{i_1, i_2, \cdots, i_m \in \{1,2\}} f_{i_1 \cdots i_m}(x) \theta^{i_1} \cdot \theta^{i_2} \cdots \theta^{i_m} \tag{2.2}$$

denote the action of the tensor $\mathbf{f}$ on $\boldsymbol{\theta}^m$.

The X-ray transform of $\mathbf{f}$ (assumed extended by 0 outside Ω) is given by

$$X\mathbf{f}(x, \boldsymbol{\theta}) := \int_{-\infty}^{\infty} \langle \mathbf{f}(x + t\boldsymbol{\theta}), \boldsymbol{\theta}^m \rangle dt, \quad (x, \boldsymbol{\theta}) \in \Gamma \times \mathbb{S}^1. \tag{2.3}$$

If lines $L_{(\beta,\theta)} := \{e^{\mathrm{i}\beta}+se^{\mathrm{i}\theta} : \ s \in \mathbb{R}\}$ are parameterized in coordinates $\{(e^{\mathrm{i}\beta}, e^{\mathrm{i}\theta}) : \beta, \theta \in (-\pi, \pi]\}$ on $\Gamma \times \mathbb{S}^1$, then

$$X\mathbf{f}(e^{\mathrm{i}\beta}, e^{\mathrm{i}\theta}) = \int_{-\infty}^{\infty} \langle \mathbf{f}(e^{\mathrm{i}\beta} + se^{\mathrm{i}\theta}), \boldsymbol{\theta}^m \rangle ds \tag{2.4}$$

is understood as a function on the torus.

Since $L_{(\beta,\theta)} = L_{(2\theta-\beta-\pi,\theta)} = L_{(\beta,\theta+\pi)} = L_{(2\theta-\beta-\pi,\theta+\pi)}$, the set of lines intersecting $\overline{\Omega}$ are quadruply covered when $(e^{\mathrm{i}\beta}, e^{\mathrm{i}\theta})$ ranges over the entire torus $\Gamma \times \mathbb{S}^1$. Moreover, the following symmetries are satisfied,

$$X\mathbf{f}(e^{\mathrm{i}\beta}, e^{\mathrm{i}\theta}) = (-1)^m X\mathbf{f}(e^{\mathrm{i}\beta}, e^{\mathrm{i}(\theta+\pi)}), \text{ and} \tag{2.5}$$

$$X\mathbf{f}(e^{\mathrm{i}\beta}, e^{\mathrm{i}\theta}) = (-1)^m X\mathbf{f}(e^{\mathrm{i}(2\theta-\beta-\pi)}, e^{\mathrm{i}(\theta+\pi)}), \text{ for } (e^{\mathrm{i}\beta}, e^{\mathrm{i}\theta}) \in \Gamma \times \mathbb{S}^1; \tag{2.6}$$

see Figure 1 below.

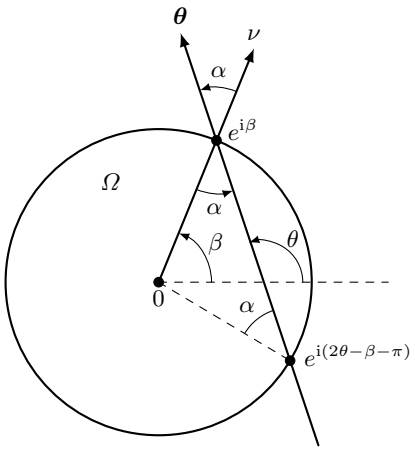

Fig. 1. Fan-beam coordinates: $e^{\mathrm{i}\beta} \in \Gamma$, $e^{\mathrm{i}\theta} \in \mathbb{S}^1$, and $\boldsymbol{\theta} = (\cos\theta, \sin\theta)$.

We consider the partition of the torus into three parts: the "outflux" part

$$\Gamma_+ := \left\{(e^{\mathrm{i}\beta}, e^{\mathrm{i}(\beta+\alpha)}) \in \Gamma \times \mathbb{S}^1 : \ \beta \in (-\pi, \pi], \ |\alpha| < \frac{\pi}{2}\right\}, \tag{2.7}$$

the "influx" part

$$\Gamma_- := \left\{(e^{\mathrm{i}\beta}, e^{\mathrm{i}(\beta+\alpha)}) \in \Gamma \times \mathbb{S}^1 : \ \beta \in (-\pi, \pi], \ \frac{\pi}{2} < |\alpha| \leq \pi\right\}, \tag{2.8}$$

and the (Lebesgue negligible) variety $\Gamma_0 := (\Gamma \times \mathbb{S}^1) \setminus (\Gamma_+ \cup \Gamma_-)$ parameterizing the tangent lines to the circle; see Figure 1.

If each component $f_{i_1 \ldots i_m} \in L^p(\Omega)$, $p \geq 1$, then $X\mathbf{f}$ may not be in $L^p(\Gamma \times \mathbb{S}^1)$. However, if (2.1) is satisfied, then $X\mathbf{f} \in L^p(\Gamma \times \mathbb{S}^1)$; see Proposition 1 for the case

of interest $p = 2$. (It can be shown that (2.1) can be relaxed by replacing the vanishing near the boundary with $\mathbf{f}$ having an L^{2p} regularity near the boundary.)

The characterization result in [17] and the proof in Section 3 hold for the larger class $L^1_0(\mathbf{S}^m; \Omega)$ of tensors with integrable components satisfying (2.1). It gives necessary and sufficient conditions for a function $g \in L^1(\Gamma \times \mathbb{S}^1)$ to satisfy

$$g = \begin{cases} X\mathbf{f}, & \text{on } \Gamma_+, \\ -X\mathbf{f}, & \text{on } \Gamma_-, \end{cases} \tag{2.9}$$

for some tensor $\mathbf{f}$.

The characterization is given in terms of the Fourier coefficients

$$g_{n,k} := \frac{1}{(2\pi)^2} \int_{-\pi}^{\pi} \int_{-\pi}^{\pi} g(e^{\mathrm{i}\beta}, e^{\mathrm{i}\theta}) e^{-\mathrm{i}n\theta} e^{-\mathrm{i}k\beta} d\theta d\beta, \ n, k \in \mathbb{Z} \tag{2.10}$$

of g on the lattice $\mathbb{Z} \times \mathbb{Z}$. where the two indexes play a different role. Throughout, the first index is the Fourier mode in the angular variable on $\mathbb{S}^1$, and we call it an *angular mode*. The second index is the mode in the boundary variable on Γ, and we call it a *boundary mode*.

The change of parity in the order of the tensor propagates to the statements of the results. For the sake of clarity, in this paper we only present the even order case.

If m is even, g in (2.9)satisfy the symmetry relation

$$g(e^{\mathrm{i}\beta}, e^{\mathrm{i}\theta}) = g(e^{\mathrm{i}(2\theta-\beta-\pi)}, e^{\mathrm{i}(\theta+\pi)}), \text{ for a.e. } (e^{\mathrm{i}\beta}, e^{\mathrm{i}\theta}) \in \Gamma \times \mathbb{S}^1, \tag{2.11}$$

and let $L^p_{\text{sym}}(\Gamma \times \mathbb{S}^1)$ denote the space of p-integrable functions g on the torus satisfying (2.11). Since $\left(e^{\mathrm{i}\beta}, e^{\mathrm{i}\theta}\right)$ and $\left(e^{\mathrm{i}(2\theta-\beta-\pi)}, e^{\mathrm{i}(\theta+\pi)}\right)$ are either both in Γ_+, or both in Γ_-, we can consider the spaces $L^1_{\text{sym}}(\Gamma_\pm)$ of integrable functions on the half-tori satisfying (2.11). Clearly, $g \in L^p_{\text{sym}}(\Gamma \times \mathbb{S}^1)$ if and only if its restrictions $g|_{\Gamma_\pm} \in L^p_{\text{sym}}(\Gamma_\pm)$. Moreover, since g in (2.9) is odd with respect to the angular variable:

$$g(e^{\mathrm{i}\beta}, e^{\mathrm{i}\theta}) = -g(e^{\mathrm{i}\beta}, e^{\mathrm{i}(\theta+\pi)}). \tag{2.12}$$

Let us consider the subspace $L^p_{\text{sym,odd}}(\Gamma \times \mathbb{S}^1)$ of functions in $L^p_{\text{sym}}(\Gamma \times \mathbb{S}^1)$, which, in addition to satisfying (2.11), they also satisfy (2.12).

In [17, Theorem 2.1] the following range characterization is given for even order tensors. The statement below leaves out the non-unique characterization of the inversion for tensors of order $m \geq 2$, which we do not use here.

Theorem 1. *(i) Let $m \geq 0$ be even and $\mathbf{f} \in L^1_0(\mathbf{S}^m; \Omega)$ be a real valued, integrable symmetric tensor field of order m satisfying* (2.1)*. If $g \in L^1_{\text{sym,odd}}(\Gamma \times \mathbb{S}^1)$ satisfies*

$$g = X\mathbf{f} \text{ on } \Gamma_+ (\text{ and } g = -X\mathbf{f} \text{ on } \Gamma_-),$$

then its Fourier coefficients $\{g_{n,k}\}_{n,k\in\mathbb{Z}}$ satisfy the following conditions:

$$\textit{Oddness}: \quad g_{n,k} = 0, \qquad \textit{for all } \text{even } n \in \mathbb{Z}, \textit{ and all } k \in \mathbb{Z}; \tag{2.13}$$

$$\textit{Conjugacy}: \quad g_{-n,-k} = \overline{g_{n,k}}, \qquad \textit{for all } n, k \in \mathbb{Z}; \tag{2.14}$$

$$\textit{Symmetry}: \quad g_{n,k} = (-1)^{n+k} g_{n+2k,-k}, \quad \textit{for all } n, k \in \mathbb{Z}; \tag{2.15}$$

$$\textit{Moments}: \quad g_{n,k} = (-1)^k g_{n+2k,-k}, \qquad \textit{for all } \text{odd } n \leq -(m+1), \textit{ and all } k \leq 0. \tag{2.16}$$

(ii) Let $\{g_{n,k}\}$ *be given for all* odd $n \leq -1$*, and* $k \in \mathbb{Z}$ *such that*

$$\sum_{\substack{n\leq -1\\ n:\,\text{odd}}} \langle n\rangle^2 \sum_{k=-\infty}^{\infty} |g_{n,k}| < \infty, \quad \textit{and} \quad \sum_{k=-\infty}^{\infty} \langle k\rangle^{1+\mu} \sum_{\substack{n\leq -1\\ n:\,\text{odd}}} |g_{n,k}| < \infty, \tag{2.17}$$

for some $1 \geq \mu > 1/2$*.*

If $\{g_{n,k}\}$ *satisfy* (2.15) *and* (2.16)*, then there exists a real valued* $\mathbf{f} \in C^{\mu}(\mathbf{S}^m; \Omega)$ *(non-unique if* $m \geq 2$*), such that the mapping*

$$(\Gamma \times \mathbb{S}^1) \ni (e^{\mathrm{i}\beta}, e^{\mathrm{i}\theta}) \longmapsto 2\,\mathbb{R}\mathrm{e}\left\{ \sum_{\substack{n\leq -1\\ n:\,\text{odd}}} \sum_{k\in\mathbb{Z}} g_{n,k} e^{\mathrm{i}n\theta} e^{\mathrm{i}k\beta} \right\} \tag{2.18}$$

defines a function in $L^1_{\text{sym,odd}}(\Gamma \times \mathbb{S}^1)$*, which coincides with* $X\mathbf{f}$ *on* Γ_+ *(and with* $-X\mathbf{f}$ *on* Γ_-*).*

The constraints (2.13) are due to the angularly-odd extension (2.9) to the entire torus. The conjugacy constraints (2.14) are due to the reality of the tensor. The symmetry constraints (2.15) merely account for each line being doubly parametrized in Γ_+, and they are shared by any function on the torus satisfying the symmetry (2.11); see [17, Lemma A.2] for details. The moment constraints (2.16) are due to the nature of the operator (integration) along the line in the definition of the X-ray transform. In the next section we present a new proof of (2.16), which does not use the theory of A-analytic maps.

3 An elementary proof of the moment conditions

In this section we present a new proof of (2.16), which does not use tools from the theory of A-analytic maps.

The starting point is Pantyukhina's result in [12], which extends the original GGHL characterization from 0 order tensors to arbitrary order tensors. The set of lines in [12] are parametrized by points on the tangent bundle $T\mathbb{S}^1 = \{(x, \boldsymbol{\theta}) | \boldsymbol{\theta} \in \mathbb{S}^1, x \cdot \boldsymbol{\theta} = 0\}$ of the unit circle. To distinguish from the parametrization of lines by points on a torus we use the notation

$$I\mathbf{f}(x, \boldsymbol{\theta}) := \int_{-\infty}^{\infty} \langle \mathbf{f}(x + t\boldsymbol{\theta}), \boldsymbol{\theta}^m \rangle dt, \quad (x, \boldsymbol{\theta}) \in T\mathbb{S}^1, \tag{3.1}$$

where $\mathbf{f}$ is extended by 0 outside Ω. In two dimensions, Pantyukhina's result states:

Theorem 2 ([12]). *Let* $\varphi \in \mathcal{S}(T\mathbb{S}^1)$ *be a rapidly decaying function on* $T\mathbb{S}^1$*. Then* $\varphi = I\mathbf{f}$ *for some symmetric* m*-tensor field* $\mathbf{f} \in \mathcal{S}(\mathbb{R}^2)$*, if and only if*

1. $\varphi(x, -\boldsymbol{\theta}) = (-1)^m \varphi(x, \boldsymbol{\theta})$ *and*

2. *for every integer $k \geq 0$, there exist homogeneous polynomials P_i^k of degree k, such that*

$$\int_{-\infty}^{\infty} s^k \varphi(s\boldsymbol{\theta}^{\perp}, \boldsymbol{\theta}) ds = \sum_{i=0}^{m} P_i^k(\cos\theta, \sin\theta) \cos^i\theta \sin^{m-i}\theta. \tag{3.2}$$

Below, we revisit the necessity part of Theorem 2 adapted to functions on the torus. For a tensor $\mathbf{f}$ supported in the unit disc, the X-ray of $\mathbf{f}$ with lines parameterized on $\Gamma \times \mathbb{S}^1$ is connected to the X-ray of $\mathbf{f}$ with lines parameterized on $T\mathbb{S}^1$ by

$$X\mathbf{f}(e^{\mathrm{i}\beta}, e^{\mathrm{i}(\alpha+\beta)}) = I\mathbf{f}(\sin\alpha\, e^{\mathrm{i}(\alpha+\beta-\frac{\pi}{2})}, e^{\mathrm{i}(\alpha+\beta)}) \text{ for } |\alpha| \leq \frac{\pi}{2} \text{ and } \beta \in (-\pi, \pi]. \tag{3.3}$$

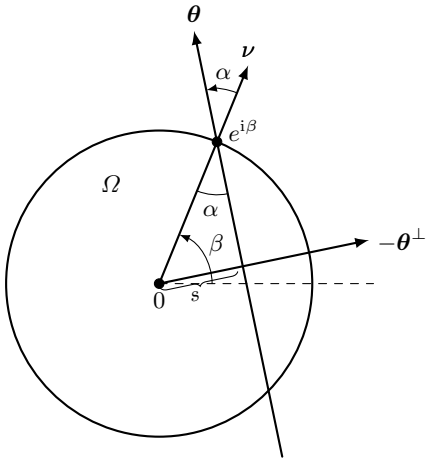

Fig. 2. $e^{\mathrm{i}\beta} \in \Gamma$, $\boldsymbol{\theta} = (\cos\theta, \sin\theta)$, $e^{\mathrm{i}\theta} = e^{\mathrm{i}(\alpha+\beta)}$, $-\boldsymbol{\theta}^{\perp} = e^{\mathrm{i}(\alpha+\beta-\frac{\pi}{2})}$.

To bring Pantyukhina's moment conditions (3.2) closer to our needs, we also recast them as orthogonality conditions.

Theorem 3. *Let $\mathbf{f} \in L^1_0(\mathbf{S}^m; \Omega)$ be a real valued, integrable symmetric m-tensor field satisfying* (2.1)*, and $h \in L^1(\Gamma \times \mathbb{S}^1)$ be defined by*

$$h := X\mathbf{f} + \begin{cases} X\mathbf{f} & \text{on } \Gamma_+, \\ -X\mathbf{f} & \text{on } \Gamma_- \end{cases} = \begin{cases} 2\,[X\mathbf{f}] & \text{on } \Gamma_+, \\ 0 & \text{on } \Gamma_-. \end{cases} \tag{3.4}$$

Then, for each $p \in \mathbb{Z}$, $p \geq 0$,

$$\int_{-\pi}^{\pi} \int_{-\pi}^{\pi} e^{\mathrm{i}n(\beta+\alpha)} (\sin\alpha)^p (\cos\alpha)\, h(e^{\mathrm{i}\beta}, e^{\mathrm{i}(\alpha+\beta)})\, d\alpha\, d\beta = 0, \text{ for all} \tag{3.5}$$

(i) $n \in \mathbb{Z}$ with $m + p - n$ odd, or
(ii) $n \in \mathbb{Z}$ with $|n| > m + p$ and $m + p - n$ even.

Proof. Since $\mathbf{f}$ is supported in the unit disc, the integration over the line reduces to the integration over the interval $[-1,1]$ regardless of the orientation of the line.

$$\begin{aligned}
\int_{-1}^{1} s^p I\mathbf{f}(s\,e^{\mathrm{i}(\theta-\frac{\pi}{2})}, e^{\mathrm{i}\theta})\,ds &= \int_{-1}^{1} s^p \int_{-1}^{1} \sum_{j=0}^{m} f_j(se^{\mathrm{i}(\theta-\frac{\pi}{2})} + te^{\mathrm{i}\theta})(\cos\theta)^{m-j}(\sin\theta)^j dtds \\
&= \sum_{j=0}^{m} \int_{-1}^{1}\int_{-1}^{1} (x_2\cos\theta - x_1\sin\theta)^p f_j(x_1,x_2)(\cos\theta)^{m-j}(\sin\theta)^j dx_1dx_2 \\
&= \sum_{j=0}^{m}\sum_{k=0}^{p} c_{j,p,k}(\cos\theta)^{m+p-(j+k)}(\sin\theta)^{j+k} \\
&= \sum_{j=0}^{m}\sum_{k=0}^{p} c_{j,p,k}\left(\frac{e^{\mathrm{i}\theta}+e^{-\mathrm{i}\theta}}{2}\right)^{m+p-(j+k)}\left(\frac{e^{\mathrm{i}\theta}-e^{-\mathrm{i}\theta}}{2\mathrm{i}}\right)^{j+k} \\
&= 2^{-m-p}e^{-\mathrm{i}\theta(m+p)}\sum_{j=0}^{m}\sum_{k=0}^{p}(-\mathrm{i})^{j+k}c_{j,p,k}Q_{m+p,j+k}(e^{2\mathrm{i}\theta}),
\end{aligned}$$

where $c_{j,p,k} = \binom{p}{k}\int_{-1}^{1}\int_{-1}^{1} f_j(x_1,x_2)(-1)^k x_1^k x_2^{p-k}\,dx_1\,dx_2$, and

$$Q_{r.k}(t) = (t+1)^{r-k}\,(t-1)^k\,,\ \text{for } 0\le k\le r. \tag{3.6}$$

Since $\{Q_{r,k}(t)\}_{k=0}^{r}$ form a basis for the space of polynomials of degree r (e.g., see [17, Lemma A.I]), the map $\zeta\mapsto\zeta^{m+p}\displaystyle\int_{\mathbb{R}} s^p I\mathbf{f}(s\zeta e^{-\mathrm{i}\frac{\pi}{2}},\zeta)ds$ is a polynomial of degree $2(m+p)$ in $\zeta\in\mathbb{C}$ with even powers only. In particular, we get the orthogonality (in $L^2(\mathbb{S}^1)$) conditions:

$$\int_{-\pi}^{\pi} e^{\mathrm{i}\theta(m+p-q)}\int_{-1}^{1} s^p I\mathbf{f}(s\,e^{\mathrm{i}(\theta-\frac{\pi}{2})}, e^{\mathrm{i}\theta})\,ds\,d\theta = 0,$$

$$\begin{cases}\text{for } q<0, \text{ or } q>2(m+p),\\ \text{or for } 1\le q\le 2(m+p)-1, \text{ and } q \text{ odd.}\end{cases}$$

By setting $n=m+p-q$,

$$\int_{-\pi}^{\pi} e^{\mathrm{i}n\theta}\int_{-1}^{1} s^p I\mathbf{f}(s\,e^{\mathrm{i}(\theta-\frac{\pi}{2})}, e^{\mathrm{i}\theta})\,ds\,d\theta = 0,$$

$$\begin{cases}\text{for } |n|>m+p,\\ \text{or for } |n|\le m+p, \text{ and } m+p-n \text{ is odd.}\end{cases}$$

Thus,

$$\int_{-\pi}^{\pi} e^{\mathrm{i}n\theta}\int_{-1}^{1} s^p I\mathbf{f}(s\,e^{\mathrm{i}(\theta-\frac{\pi}{2})}, e^{\mathrm{i}\theta})\,ds\,d\theta = 0,\ \text{for all} \tag{3.7}$$

(i) $n \in \mathbb{Z}$ with $m+p-n$ odd, or
(ii) $n \in \mathbb{Z}$ with $|n| > m+p$ and $m+p-n$ even.

For each $e^{\mathrm{i}\beta} \in \Gamma$, let $\alpha \in \left(-\frac{\pi}{2}, \frac{\pi}{2}\right)$ be the angle measured counter-clockwise from the outer unit normal at $e^{\mathrm{i}\beta} \in \Gamma$; see Figure 2. By the change of variables $s = \sin\alpha$ in (3.7), and using the relation (3.3), the moment conditions become

$$\begin{aligned} 0 &= \int_{-\pi}^{\pi} e^{\mathrm{i}n(\beta+\alpha)} \int_{-\frac{\pi}{2}}^{\frac{\pi}{2}} (\sin\alpha)^p I\mathbf{f}(\sin\alpha\, e^{\mathrm{i}(\alpha+\beta-\frac{\pi}{2})}, e^{\mathrm{i}(\alpha+\beta)})\, \cos\alpha\, d\alpha\, d\beta \\ &= \int_{-\pi}^{\pi} e^{\mathrm{i}n(\beta+\alpha)} \int_{-\frac{\pi}{2}}^{\frac{\pi}{2}} (\sin\alpha)^p\, \cos\alpha\, X\mathbf{f}(e^{\mathrm{i}\beta}, e^{\mathrm{i}(\alpha+\beta)})\, d\alpha\, d\beta. \end{aligned}$$

Since g in (3.4) vanishes on Γ_-, i.e., $g(e^{\mathrm{i}\beta}, e^{\mathrm{i}(\alpha+\beta)}) = 0$, for all $\beta \in (-\pi, \pi]$ and $\frac{\pi}{2} < |\alpha| \leq \pi$, one obtains (3.5). This ends the proof of Theorem 2.

The moment conditions (2.16) in Theorem 1 follow as a corollary to Theorem 2. Since the odd angular modes are preserved upon addition with the modes of the angularly even function $X\mathbf{f}$, suffices to prove (2.16) for the function h in (3.4).

Corollary 1 *Let $\mathbf{f} \in L^1_0(\mathbf{S}^m; \Omega)$ be a real valued, integrable symmetric tensor field of even order $m \geq 0$ satisfying* (2.1)*, and $h \in L^1_{\text{sym}}(\Gamma \times \mathbb{S}^1)$ be defined by* (3.4)*. Then its Fourier coefficients $\{h_{n,k}\}_{n,k\in\mathbb{Z}}$ satisfy*

$$h_{n,k} = (-1)^k h_{n+2k,-k}, \text{ for all odd } n \leq -m-1, \text{ and all } k \leq 0.$$

Proof. We use (3.5) in Theorem 3 part (ii) with $|n| > m+p$. Since m is even, $m+(p-n)$ and $p-n$ have the same parity. We consider two separate cases: p and n both even, and p and n both odd.

Case 1: $|n| > m+p$, and p and n both even.

Since $\operatorname{span}\left\{\cos\alpha\,(\sin\alpha)^{2j},\ 0 \leq j \leq k\right\} = \operatorname{span}\left\{\cos[(2j+1)\alpha],\ 0 \leq j \leq k\right\}$ for all $k \geq 0$, the orthogonality in (3.5) for this case becomes

$$\begin{aligned} 0 &= \int_{-\pi}^{\pi}\int_{-\pi}^{\pi} e^{\mathrm{i}n(\beta+\alpha)} \cos[(p+1)\alpha]\; h(e^{\mathrm{i}\beta}, e^{\mathrm{i}(\alpha+\beta)})\, d\alpha\, d\beta \\ &= \frac{1}{2}\int_{-\pi}^{\pi}\int_{-\pi}^{\pi} e^{\mathrm{i}n(\beta+\alpha)} e^{\mathrm{i}(p+1)\alpha} h(e^{\mathrm{i}\beta}, e^{\mathrm{i}(\alpha+\beta)})\, d\alpha\, d\beta \\ &\quad + \frac{1}{2}\int_{-\pi}^{\pi}\int_{-\pi}^{\pi} e^{\mathrm{i}n(\beta+\alpha)} e^{-\mathrm{i}(p+1)\alpha} h(e^{\mathrm{i}\beta}, e^{\mathrm{i}(\alpha+\beta)})\, d\alpha\, d\beta. \end{aligned} \tag{3.8}$$

In the last equality of (3.8) let us consider the first term,

$$\begin{aligned} &\int_{-\pi}^{\pi}\int_{-\pi}^{\pi} e^{\mathrm{i}n(\beta+\alpha)} e^{\mathrm{i}(p+1)\alpha} h(e^{\mathrm{i}\beta}, e^{\mathrm{i}(\alpha+\beta)})\, d\alpha\, d\beta \\ &\overset{\alpha=\theta-\beta}{=\!=\!=} \int_{-\pi}^{\pi}\int_{-\pi}^{\pi} e^{\mathrm{i}\theta(n+p+1)} e^{-\mathrm{i}(p+1)\beta} h(e^{\mathrm{i}\beta}, e^{\mathrm{i}\theta})\, d\theta\, d\beta = (2\pi)^2 h_{-n-p-1,p+1}. \end{aligned} \tag{3.9}$$

Similarly, the last term in (3.8) rewrites

$$\int_{-\pi}^{\pi}\int_{-\pi}^{\pi} e^{\mathrm{i}n(\beta+\alpha)}e^{-\mathrm{i}(p+1)\alpha}h(e^{\mathrm{i}\beta},e^{\mathrm{i}(\alpha+\beta)})\,d\alpha\,d\beta$$
$$\overset{\alpha=\theta-\beta}{=\!=\!=} \int_{-\pi}^{\pi}\int_{-\pi}^{\pi} e^{\mathrm{i}\theta(n-p-1)}e^{\mathrm{i}(p+1)\beta}h(e^{\mathrm{i}\beta},e^{\mathrm{i}\theta})\,d\theta\,d\beta = (2\pi)^2 h_{-n+p+1,-p-1}. \tag{3.10}$$

Using (3.9), and (3.10), the expression in (3.8) yields

$$h_{-n-p-1,p+1} = -h_{-n+p+1,-p-1}, \quad \text{for } n,p \text{ even, } |n|>m+p, \text{ and } p\geq 0. \tag{3.11}$$

By setting $k=-p-1$ (odd) and $|n|\geq m+p+2 = m-k+1$, and $r=-n-k$ (odd), we obtain,

$$h_{r,k} = (-1)^k h_{r+2k,-k}, \text{ for all odd } k\leq -1, \text{ and all odd } r\leq -m-1. \tag{3.12}$$

Case 2: We consider (3.5) for all $p\geq 0,\ |n|>m+p$, and p and n both odd.

Since $\operatorname{span}\left\{\cos\alpha\,(\sin\alpha)^{2j+1},\ 0\leq j\leq k\right\} = \operatorname{span}\left\{\sin[(2j+2)\alpha],\ 0\leq j\leq k\right\}$ for all $k\geq 0$, the orthogonality in (3.5) for this case becomes

$$\begin{aligned} 0 &= \int_{-\pi}^{\pi}\int_{-\pi}^{\pi} e^{\mathrm{i}n(\beta+\alpha)}\sin[(p+1)\alpha]\ h(e^{\mathrm{i}\beta},e^{\mathrm{i}(\alpha+\beta)})\,d\alpha\,d\beta \\ &= \frac{1}{2i}\int_{-\pi}^{\pi}\int_{-\pi}^{\pi} e^{\mathrm{i}n(\beta+\alpha)}e^{\mathrm{i}(p+1)\alpha}h(e^{\mathrm{i}\beta},e^{\mathrm{i}(\alpha+\beta)})\,d\alpha\,d\beta \\ &\quad -\frac{1}{2i}\int_{-\pi}^{\pi}\int_{-\pi}^{\pi} e^{\mathrm{i}n(\beta+\alpha)}e^{-\mathrm{i}(p+1)\alpha}h(e^{\mathrm{i}\beta},e^{\mathrm{i}(\alpha+\beta)})\,d\alpha\,d\beta. \end{aligned} \tag{3.13}$$

Using (3.9) and (3.10), the expression in (3.13) yields

$$h_{-n-p-1,p+1} = h_{-n+p+1,-p-1}, \quad \text{for } n,p \text{ odd, } |n|>m+p, \text{ and } p\geq 0.$$

By setting $k=-p-1$ (even), $|n|\geq m+p+2 = m-k+1$, and $r=-n-k$ (odd), we obtain

$$h_{r,k} = (-1)^k h_{r+2k,-k}, \text{ for all even } k\leq -2, \text{ and all odd } r\leq -m-1. \tag{3.14}$$

In summary (3.12) and (3.14), yields

$$h_{r,k} = (-1)^k h_{r+2k,-k}, \text{ for all } k\leq -1, \text{ and all odd } r\leq -m-1.$$

Since the relation above trivially holds for $k=0$, we showed that the moment conditions (2.16) hold.

4 The algebraic range of the X-ray transform of even order tensors

In this section the square integrability of $X\mathbf{f}$ is needed. The following result gives a sufficient condition on $\mathbf{f}$ to ensure square integrability of $X\mathbf{f}$.

Proposition 1 *Let the components of* $\mathbf{f} \in L^2_0(\mathbf{S}^m; \Omega)$ *satisfy*

$$\text{supp } f_{i_1 \dots i_m} \subset \{z \in \Omega : |z| \leq \sqrt{1-\delta^2}\},\ 0 < \delta < 1. \tag{4.1}$$

Then $X\mathbf{f} \in L^2(\Gamma \times \mathbb{S}^1)$ *and, thus, the extension* (2.9) *is square integrable on* $\Gamma \times \mathbb{S}^1$.

Proof. Since $\mathbf{f}$ is symmetric, for any m-tuple $(i_1, \cdots, i_m) \in \{1,2\}^m$ such that 2 occurs exactly k times (and 1 occurs $m-k$ times), the component $f_{i_1 \dots i_m}$ satisfies

$$f_{i_1 \dots i_m} = f_{\underbrace{1 \cdots 1}_{m-k} \underbrace{2 \cdots 2}_{k}} =: \tilde{f}_k. \tag{4.2}$$

Since there are $\binom{m}{k}$ many m-tuples $(i_1, i_2, \cdots, i_m)$ that contain exactly k many $2's$,

$$\begin{aligned}\langle \mathbf{f}(z), \boldsymbol{\theta}^m \rangle &\overset{(4.2)}{=\!=} \sum_{k=0}^{m} \binom{m}{k} \tilde{f}_k(z)\ (\cos\theta)^{(m-k)} (\sin\theta)^k \\ &= e^{-\mathrm{i}m\theta} 2^{-m} \sum_{k=0}^{m} (-\mathrm{i})^k \binom{m}{k} \tilde{f}_k(z)\ Q_{m,k}(e^{2\mathrm{i}\theta}),\end{aligned}$$

where $Q_{m,k}$ are the polynomials in (3.6).

Since the order of the tensor is even, say $m = 2l$, for some $l \geq 0$, we obtained

$$\langle \mathbf{f}, \boldsymbol{\theta}^m \rangle = \sum_{k=0}^{l} f_{2k} e^{-\mathrm{i}(2k)\theta} + \sum_{k=1}^{l} f_{-2k} e^{\mathrm{i}(2k)\theta}, \tag{4.3}$$

where f_k's are in a one-to-one correspondence with $\tilde{f}_k$, and thus with $f_{i_1 \cdots i_m}$; see [17, Lemma A.1]. Since all the components $f_{i_1 \dots i_m} \in L^2_0(\Omega)$ satisfy the support condition (4.1), $f_{2k} \in L^2_0(\Omega)$ also satisfies the same support condition (4.1), for all $-l \leq k \leq l$.

Using the identity (4.3), the X-ray transform of $\mathbf{f}$ (with components extended by 0 outside Ω) writes as $X\mathbf{f} = \sum_{k=-l}^{l} X_k(f_{2k})$, where X_k is the weighted ray transform

$$X_k(f)(e^{\mathrm{i}\beta}, e^{\mathrm{i}\theta}) := \int_{-\infty}^{\infty} f(e^{\mathrm{i}(\beta-\theta)} + t) e^{-\mathrm{i}2k\theta} dt.$$

For any $f \in L^2_0(\Omega)$ satisfying the support condition (4.1), we show next that $X_k(f) \in L^2(\Gamma \times \mathbb{S}^1)$. In the estimate below (fourth equality) we denote by f_θ the function obtained from f by a rotation of the domain by an angle θ, $f_\theta(z) := f(ze^{\mathrm{i}\theta})$.

Note that $\|f_\theta\|^2_{L^2(\Omega)} = \|f\|^2_{L^2(\Omega)}$.

$$\begin{aligned}
\|X_k f\|^2{}_{L^2(\Gamma\times\mathbb{S}^1)} &= \frac{1}{(2\pi)^2}\int_{-\pi}^{\pi}\int_{-\pi}^{\pi}|X_k f(e^{\mathrm{i}\beta},e^{\mathrm{i}\theta})|^2 d\beta d\theta \\
&= \frac{1}{(2\pi)^2}\int_{-\pi}^{\pi}\int_{-\pi}^{\pi}\left|\int_{-\infty}^{\infty} f(e^{\mathrm{i}\beta}+te^{\mathrm{i}\theta})e^{-2\mathrm{i}k\theta}dt\right|^2 d\beta d\theta \\
&= \frac{1}{(2\pi)^2}\int_{-\pi}^{\pi}\int_{-\pi}^{\pi}\left|\int_{-2}^{2} f(e^{\mathrm{i}\beta}+te^{\mathrm{i}\theta})e^{-2\mathrm{i}k\theta}dt\right|^2 d\beta d\theta \\
&\leq 4\frac{1}{(2\pi)^2}\int_{-\pi}^{\pi}\int_{-\pi}^{\pi}\int_{-2}^{2}|f(e^{\mathrm{i}\beta}+te^{\mathrm{i}\theta})|^2 dt d\beta d\theta \\
&= \frac{1}{\pi^2}\int_{-\pi}^{\pi}\int_{-\pi}^{\pi}\int_{-2}^{2}|f_\theta(e^{\mathrm{i}(\beta-\theta)}+t)|^2 dt d\beta d\theta \\
&\overset{\alpha=\beta-\theta}{=\!=\!=} \frac{2}{\pi^2}\int_{-\pi}^{\pi}\int_{-\pi/2}^{\pi/2}\int_{-2}^{2}|f_\theta(e^{\mathrm{i}\alpha}+t)|^2 dt d\alpha d\theta \\
&\overset{s=\sin\alpha}{=\!=\!=} \frac{2}{\pi^2}\int_{-\pi}^{\pi}\int_{-2}^{2}\int_{-1}^{1}\frac{|f_\theta(\sqrt{1-s^2}+t+\mathrm{i}s)|^2}{\sqrt{1-s^2}} ds dt d\theta \\
&\overset{u=t+\sqrt{1-s^2}}{=\!=\!=\!=} \frac{2}{\pi^2}\int_{-\pi}^{\pi}\int_{-1}^{1}\int_{-1}^{1}\frac{|f_\theta(u+\mathrm{i}s)|^2}{\sqrt{1-s^2}} ds du d\theta,
\end{aligned} \tag{4.4}$$

where the third equality uses that Ω has diameter 2, and the last equality uses the fact that the unit disc lies inside any rotated circumscribed square.

Since $\mathrm{supp} f_\theta \subset \{z : |z| \leq \sqrt{1-\delta^2}\}$, regardless of the rotation angle θ,

$$\begin{aligned}
\|X_k f\|^2_{L^2(\Gamma\times\mathbb{S}^1)} &\leq \frac{2}{\pi^2}\int_{-\pi}^{\pi}\int_{-1}^{1}\int_{-\sqrt{1-\delta^2}}^{\sqrt{1-\delta^2}}\frac{|f_\theta(u+\mathrm{i}s)|^2}{\sqrt{1-s^2}} ds du d\theta \\
&\leq \frac{2}{\pi^2\delta}\int_{-\pi}^{\pi}\|f_\theta\|^2_{L^2(\Omega)}\, d\theta = \frac{4}{\pi\delta}\|f\|^2_{L^2(\Omega)}.
\end{aligned}$$

The constraints in Theorems 1 determine a closed subspace of $L^2(\Gamma\times\mathbb{S}^1)$, which contains the range of the X-ray transform of square integrable tensors.

Definition 1. *Let $m \geq 0$ be even. The algebraic range $AR(X)$ of the X-ray transform of symmetric m-tensors is defined by those $g \in L^2(\Gamma\times\mathbb{S}^1)$ with Fourier coefficients satisfying* (2.13)*,* (2.14)*,* (2.15) *and* (2.16)*.*

Since m is even, (2.13) yields that only the odd angular modes need be considered. To further describe the algebraic interaction between (2.14), (2.15), and (2.16), let us consider the three-set partition of $\mathbb{Z}^-_{\text{odd}}\times\mathbb{Z} = G\cup R\cup W$ (see Figure 3) introduced in [17]:

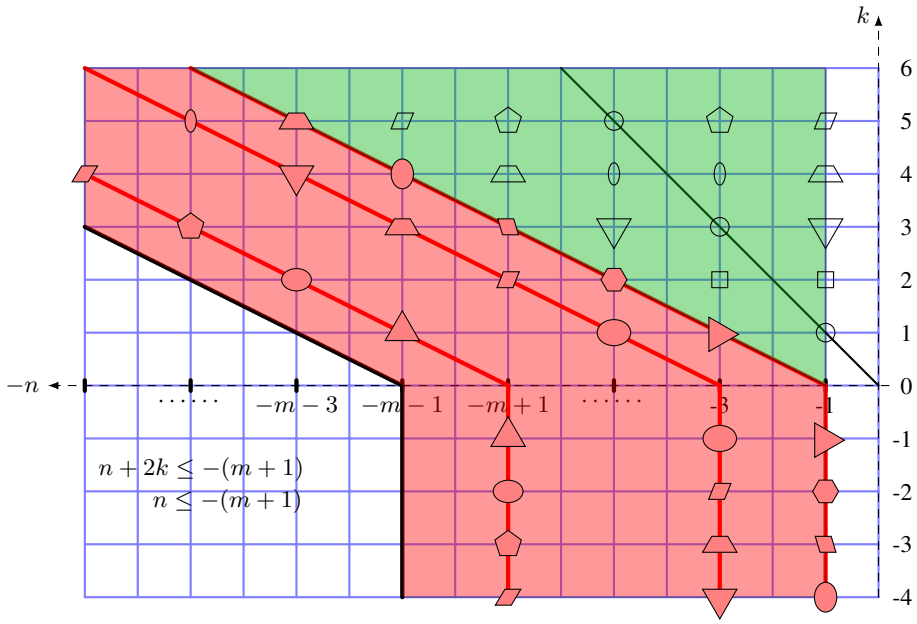

Fig. 3. An even order m-tensor field $\mathbf{f}$ is determined by the odd negative angular modes on or above the diagonal $k = -n$ (green region), and the odd negative angular modes (marked red) on the $\frac{m}{2}$ red lines $n + 2k = -(m + 1)$ for $k \geq 0$. All the odd non-positive angular modes on and below the line $n + 2k = -(m+1)$, and on and left of the line $n = -(m+1)$ vanish. For $n \geq 0$ the picture is symmetric with respect to the origin.

– the region $W := W^+ \cup W^-$, where

$$W^+ := \left\{ (n,k) \in \mathbb{Z}^-_{\text{odd}} \times \mathbb{Z}^+ \ : \text{odd } n \leq -m-1, \text{ and } 0 \leq k \leq -\frac{n+m+1}{2} \right\},$$
$$W^- := \left\{ (n,k) \in \mathbb{Z}^-_{\text{odd}} \times \mathbb{Z}^- \ : \text{odd } n \leq -m-1, \text{ and } k \leq 0 \right\}. \tag{4.5}$$

– the region $G := G_L \cup G_R \cup \Delta$, where

$$G_L := \left\{ (n,k) \in \mathbb{Z}^-_{\text{odd}} \times \mathbb{Z}^+ \ : k \geq 1 \text{ and } -2k+1 \leq n < -k, \ n \text{ odd} \right\},$$
$$G_R := \left\{ (n,k) \in \mathbb{Z}^-_{\text{odd}} \times \mathbb{Z}^+ \ : k \geq 1 \text{ and } n > -k, \ n \text{ odd} \right\}, \tag{4.6}$$
$$\Delta := \{ (-k,k) : \text{ odd } k \geq 1 \}.$$

– and, for $m \geq 2$, the region $R = R^+ \cup R^-$ with

$$R^+ := \left\{ (n,k) \in \mathbb{Z}^-_{\text{odd}} \times \mathbb{Z}^+ \ : k \geq 1, \text{ and } \ -m+1-2k \leq n \leq -1-2k, \ n \text{ odd} \right\},$$
$$R^- := \left\{ (n,k) \in \mathbb{Z}^-_{\text{odd}} \times \mathbb{Z}^- \ : k \leq 0, \text{ and } \ -m+1 \leq n \leq -1, n \text{ odd} \right\}. \tag{4.7}$$

If $m = 0$ (case considered in the numerical experiments in Section 5), then $R = \emptyset$ and $\mathbb{Z}_- \times \mathbb{Z} = W \cup G$; see Fig. 4.

Note the invariance of G under the transformation $(n,k) \mapsto (-n-2k,k)$, and that of R (for $m \geq 2$) under the transformation $(n,k) \mapsto (n+2k,-k)$. More precisely if $(n,k) \in G_L$, then $(-n-2k,k) \in G_R$, and conversely, if $(n,k) \in G_R$, then $(-n-2k,k) \in G_L$. Similarly, if $(n,k) \in R^+$, then $(n+2k,-k) \in R^-$, and conversely, if $(n,k) \in R^-$, then $(n+2k,-k) \in R^+$.

For a given integer $N \geq 1$, we also consider the finite sub-lattice I_N of points inside the rectangle $[-m+1-2N, m-1+2N] \times [-N,N]$,

$$I_N = \{(n,k) \in \mathbb{Z}_{\text{odd}} \times \mathbb{Z} : \ n \text{ odd }, |n| \leq m-1+2N, \text{ and } |k| \leq N\}. \tag{4.8}$$

In the case of even order tensors we only work with functions that are angularly-odd. For brevity, let denote

$$L^2_{\text{odd}}(\Gamma \times \mathbb{S}^1) := \left\{ g \in L^2(\Gamma \times \mathbb{S}^1) : \ g(e^{\mathrm{i}\beta}, e^{\mathrm{i}\theta}) = -g(e^{\mathrm{i}\beta}, -e^{\mathrm{i}\theta}) \right\}.$$

Following directly from (2.14), (2.15), and (2.16), $g \in L^2_{\text{odd}}(\Gamma \times \mathbb{S}^1) \cap AR(X)$ if and only if for all *odd* $n \leq -1$,

$$g_{n,k} = \begin{cases} 0, & \text{if } (n,k) \in W, \\ (-1)^{1+k} \overline{g_{-n-2k,k}}, & \text{if } (n,k) \in G, \\ (-1)^{1+k} g_{n+2k,-k}, & \text{if } (n,k) \in R. \end{cases} \tag{4.9}$$

Note also that (2.13) already implies $L^2_{\text{odd}}(\Gamma \times \mathbb{S}^1) \cap AR(X) = L^2(\Gamma \times \mathbb{S}^1) \cap AR(X)$.

The following result provides the theoretical support of the denoising method proposed in Section 5.

Theorem 4. *Let $g \in L^2_{\text{odd}}(\Gamma \times \mathbb{S}^1)$ be an angularly odd real valued function with Fourier coefficients $\{g_{n,k}\}$. For some fixed even $m \geq 0$, consider the partition $G \cup R \cup W$ of $\mathbb{Z}_- \times \mathbb{Z}$ with W in* (4.5)*, G in* (4.6)*, and R in* (4.7) *and define the new function*

$$g^*(e^{\mathrm{i}\beta}, e^{\mathrm{i}\theta}) := 2\,\mathbb{R}\mathrm{e}\left(\sum_{odd\ n \leq -1} \sum_{k=-\infty}^{\infty} g^*_{n,k} e^{\mathrm{i}n\theta} e^{\mathrm{i}k\beta} \right), \tag{4.10}$$

where

$$g^*_{n,k} = \begin{cases} 0, & \textit{if } (n,k) \in W, \\ \frac{1}{2}\left(g_{n,k} + (-1)^{1+k} \overline{g_{-n-2k,k}} \right), & \textit{if } (n,k) \in G, \\ \frac{1}{2}\left(g_{n,k} + (-1)^{1+k} g_{n+2k,-k} \right), & \textit{if } (n,k) \in R. \end{cases} \tag{4.11}$$

Then

$$g^* = \textit{argmin} \left\{ \|g-h\|^2_{L^2(\Gamma \times \mathbb{S}^1)} : \ \ h \in L^2_{\text{odd}}(\Gamma \times \mathbb{S}^1) \cap AR(X) \right\}. \tag{4.12}$$

Moreover, for any $N \geq 1$ arbitrarily fixed, the band limited approximation

$$g^*_N(e^{\mathrm{i}\beta}, e^{\mathrm{i}\theta}) := 2\,\mathbb{R}\mathrm{e}\left(\sum_{n=-m+1-2N}^{-1} \sum_{k=-N}^{N} g^*_{n,k} e^{\mathrm{i}n\theta} e^{\mathrm{i}k\beta} \right), \tag{4.13}$$

is the X-ray transform of some symmetric m-tensor in $C^1(\mathbb{S}^m; \Omega)$.

Proof. Following directly from its definition in (4.10), it is easy to see that $g^* \in AR(X) \cap L^2_{odd}(\Gamma \times \mathbb{S}^1)$. Also following directly from the definition (4.10) on the antidiagonal Δ, the Fourier coefficients of g and g^* coincide:

$$g_{-k,k} = g^*_{-k,k}, \quad \text{for odd } k \geq 0. \tag{4.14}$$

Moreover, since g is angularly odd, for all $n \in \mathbb{Z}$, $g_{2n,k} = 0$.

Now let $h \in L^2_{\text{odd}}(\Gamma \times \mathbb{S}^1) \cap AR(X)$ be arbitrary. The Fourier coefficients $h_{n,k}$ of h, then satisfy (4.9). In particular, they vanish in W. Moreover, the third condition in (4.9) also yields $h_{n,0} = 0$ for all $n \leq -1$ odd. Since g is real valued, (2.14) holds and the Fourier modes $\{g_{n,k}\}$ for $n \leq 0$ and $k \in \mathbb{Z}$ determines half the norm. We estimate:

$$\begin{aligned}
&\frac{1}{2}\|g-h\|^2_{L^2(\Gamma\times\mathbb{S}^1)} - \sum_{(n,k)\in W} |g_{n,k}|^2 - \sum_{n=-m+1}^{-1} |g_{n,0}|^2 \\
&\quad= \sum_{(n,k)\in G} |g_{n,k}-h_{n,k}|^2 + \sum_{(n,k)\in R} |g_{n,k}-h_{n,k}|^2 \\
&\quad= \sum_{(n,k)\in G_L\cup G_R} |g_{n,k}-h_{n,k}|^2 + \sum_{(-k,k)\in\Delta} |g_{-k,k}-h_{-k,k}|^2 \\
&\qquad+ \sum_{(n,k)\in R^+} |g_{n,k}-h_{n,k}|^2 + \sum_{(n,k)\in R^-} |g_{n,k}-h_{n,k}|^2 \\
&\quad\geq \sum_{(n,k)\in G_L} \left(|g_{n,k}-h_{n,k}|^2 + |g_{-n-2k,k}-h_{-n-2k,k}|^2\right) \\
&\qquad+ \sum_{(n,k)\in R^+} \left(|g_{n,k}-h_{n,k}|^2 + |g_{n+2k,-k}-h_{n+2k,-k}|^2\right) \\
&\quad= \sum_{(n,k)\in G_L} \left(|g_{n,k}-h_{n,k}|^2 + |g_{-n-2k,k}-(-1)^{1+k}\overline{h_{n,k}}|^2\right) \\
&\qquad+ \sum_{(n,k)\in R^+} \left(|g_{n,k}-h_{n,k}|^2 + |g_{n+2k,-k}-(-1)^{1+k}h_{n,k}|^2\right) \\
&\quad= \sum_{(n,k)\in G_L} \left(|g_{n,k}-h_{n,k}|^2 + |(-1)^{1+k}\overline{g_{-n-2k,k}}-h_{n,k}|^2\right) \\
&\qquad+ \sum_{(n,k)\in R^+} \left(|g_{n,k}-h_{n,k}|^2 + |(-1)^{1+k}g_{n+2k,-k}-h_{n,k}|^2\right).
\end{aligned} \tag{4.15}$$

To show that g^* is a minimizer of the functional defined by the right hand side above, we use the simple geometric fact: If $z_0, z_1 \in \mathbb{C}$, then their midpoint

$$\frac{z_0+z_1}{2} = \text{argmin}\left\{|z-z_0|^2 + |z-z_1|^2 :\ z \in \mathbb{C}\right\} \tag{4.16}$$

and the minimum value is $\frac{1}{2}|z_0-z_1|^2$.

By applying (4.16) to each term $(n,k) \in G_L \cup R^+$ in (4.15), we further estimate

$$\begin{aligned}
\frac{1}{2}\|g-h\|^2_{L^2(\Gamma\times\mathbb{S}^1)} - \sum_{(n,k)\in W}|g_{n,k}|^2 - \sum_{n=-m+1}^{-1}|g_{n,0}|^2 \\
&\geq \sum_{(n,k)\in G_L}\left(|g_{n,k}-g^*_{n,k}|^2 + |(-1)^{1+k}\overline{g_{-n-2k,k}} - g^*_{n,k}|^2\right) \\
&\quad + \sum_{(n,k)\in R^+}\left(|g_{n,k}-g^*_{n,k}|^2 + |(-1)^{1+k}g_{n+2k,-k} - g^*_{n,k}|^2\right) \\
&= \sum_{(n,k)\in G}|g_{n,k}-g^*_{n,k}|^2 + \sum_{(n,k)\in R}|g_{n,k}-g^*_{n,k}|^2 \\
&= \frac{1}{2}\|g-g^*\|^2_{L^2(\Gamma\times\mathbb{S}^1)} - \sum_{(n,k)\in W}|g_{n,k}|^2 - \sum_{n=-m+1}^{-1}|g_{n,0}|^2.
\end{aligned}$$

The next to the last equality above uses the fact in (4.14) that the anti-diagonal Fourier coefficients of g and g^* coincide.

Since the functional in (4.12) is strictly convex, g^* is the unique minimizer. Moreover, g^* is the orthogonal projection of g onto $AR(X)$.

The band limited approximation g^*_N lies in $AR(X)$ and trivially satisfies the decay condition (2.17) in the sufficiency part of Theorem 1 with $\mu = 1$. Thus, g^*_N is the X-ray transform of some symmetric tensor in $C^1(\mathbf{S}^m;\Omega)$.

Since $\lim_{N\to\infty}\|g^*-g^*_N\|_{L^2(\Gamma\times\mathbb{S}^1)} = 0$, we have also shown that $AR(X)$ is the closure in $L^2(\Gamma\times\mathbb{S}^1)$ of the range of X-ray transform of symmetric tensor in $C^1(\mathbf{S}^m;\Omega)$.

5 Numerical experiments for the 0-order case

We present three numerical examples to illustrate the effect of using the projection method in the inversion of the X-ray transform of functions of compact support in the unit disc.

In the 0-order case, recall that the region R in the partition of the lattice $\mathbb{Z}_-\times\mathbb{Z}$ is empty and, thus, $\mathbb{Z}_-\times\mathbb{Z} = W\cup G$; see Fig 4 below.

For K and N positive even integers let $\Delta\beta = 2\pi/K$, $\Delta\theta = 2\pi/N$ and

$$\begin{aligned}
\beta_\ell &= -\pi + \ell\Delta\beta, \quad 0\leq \ell < K,\\
\theta_m &= -\pi + m\Delta\theta, \quad 0\leq m < N,
\end{aligned}$$

which are equi-spaced points in the interval $[-\pi,\pi)$. In practice one is given some (noisy) data $Xf^+ = g^+ \in L^2(\Gamma_+)$ in the fan-beam coordinates, passing through $e^{\mathrm{i}\beta_\ell}\in\partial\Omega$ and going in θ_m-directions.

More precisely, our numerical experiment is processed in the following procedure.

1. We construct the discretized angularly-odd extension $g\in L^2_{\text{odd}}(\Gamma\times\mathbb{S}^1)$ in (2.9) via

$$g(e^{\mathrm{i}\beta_\ell},e^{\mathrm{i}\theta_m}) = \begin{cases} g^+(e^{\mathrm{i}\beta_\ell},e^{\mathrm{i}\theta_m}), & \text{if } (e^{\mathrm{i}\beta_\ell},e^{\mathrm{i}\theta_m})\in\Gamma_+,\\ -g^+(e^{\mathrm{i}\beta_\ell},-e^{\mathrm{i}\theta_m}), & \text{if } (e^{\mathrm{i}\beta_\ell},e^{\mathrm{i}\theta_m})\in\Gamma_-. \end{cases} \tag{5.1}$$

2. Compute the Fourier coefficients (see (2.10)) by

$$g_{n,k} = \frac{\Delta\theta\Delta\beta}{(2\pi)^2} \sum_{\ell=0}^{K-1} \sum_{m=0}^{N-1} g(e^{\mathrm{i}\beta_\ell}, e^{\mathrm{i}\theta_m}) e^{-\mathrm{i}n\theta_m} e^{-\mathrm{i}k\beta_\ell}, \quad |n| < N, |k| < K. \quad (5.2)$$

3. Denoise Xf^+ by the algebraic range condition. See (2.13), (2.14), (4.9), and Fig. 4.
   (a) $g^*_{n,k} = 0$ for non-positive even $n > -N$ (including $n = 0$) and all $|k| < K$.
   (b) $\mathbb{I}\mathrm{m}\, g^*_{-n,n} = 0$, for positive $n < \min\{K, N\}$.
   (c) $g^*_{n,k} = 0$ for $(n,k) \in W \cap \{-N < n < 0, |k| < K\}$.
   (d) For $(n,k) \in G_L \cap \{-N < n < 0\}$,

$$g^*_{n,k} = \frac{1}{2}\left(g_{n,k} + (-1)^{k+1}\overline{g_{-n-2k,k}}\right)$$

   and

$$g^*_{-n-2k,k} = (-1)^{k+1}\overline{g^*_{n,k}}$$

4. Modify $\{g^*_{n,k}\}$ as an image of Fourier coefficients of a real sequence.
   (a) $g^*_{-N-n,K-k} = 0$ for negative odd $n > -N$, and k with $0 < k < -(n+1)/2$.
   (b) Take the average of $g^*_{n,k}$ and $\overline{g^*_{-N-n,K-k}}$, i.e. they are set as

$$\tfrac{1}{2}\left(g^*_{n,k} + \overline{g^*_{-N-n,K-k}}\right)$$

   for $1 \le k < K$, $-N/2 < n \le -1$, odd n, with $-1 < n + 2k < 2K - N$.

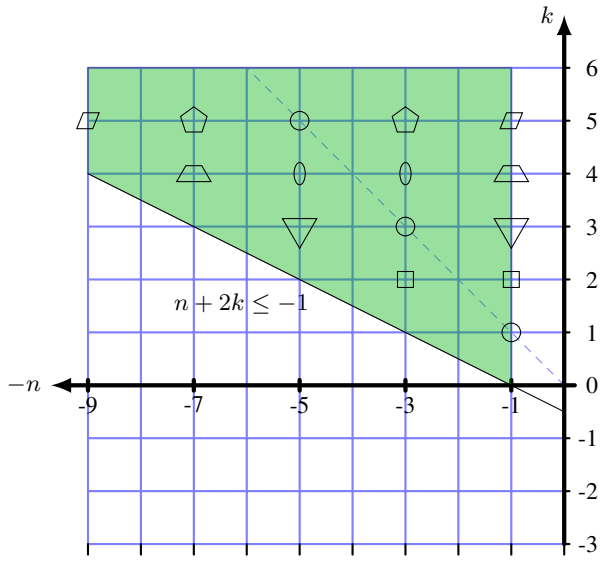

Fig. 4. The 0- tensor **f** is determined by the odd negative angular modes on or above the diagonal $k = -n$. The diagonal modes $g_{n,-n}$ are real valued. All the odd non-positive angular modes on and below the line $n + 2k = -1$ vanish.

5. Compute the denoised X-ray transform image $Xf^*_{\ell m}$ by

$$Xf^*_{\ell m} = \sum_{n=-N+1}^{-1} \sum_{k=0}^{K-1} g^*_{n,k} e^{\mathrm{i}n\theta_m} e^{\mathrm{i}k\beta_\ell}, \tag{5.3}$$

for $0 \le \ell < K$ and $0 \le m < N$ with $(e^{\mathrm{i}\beta_\ell}, e^{\mathrm{i}\theta_m}) \in \Gamma_+$.

6. Reconstruct the function f from $\{Xf^*_{\ell m}\}$.

Fig. 5 illustrates the denoised coefficients by the above procedure in $n \le 0$ and $k \ge 0$ for the case $K = N = 8$. For even n including $n = 0$, $g^*_{n,k}$ is zero by (3a). The diagonals $g^*_{-1,1}, g^*_{-3,3}, g^*_{-5,5}$, and $g^*_{-7,7}$ are real by (3b). The Greek characters recall the relation in (3d), which is numerically satisfied.

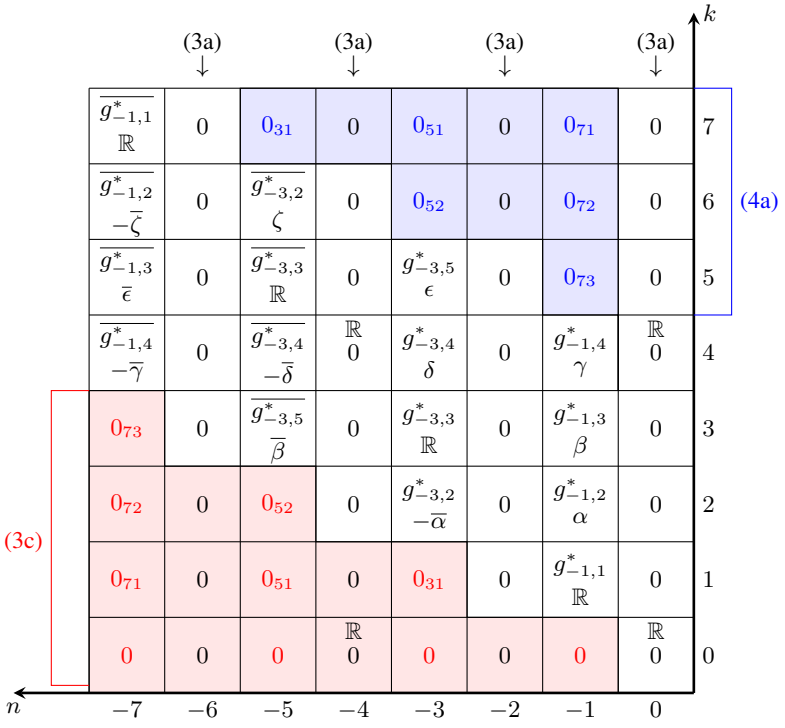

Fig. 5. Example of denoised data for $N = K = 8$. For each element, below expresses the algebraic range condition, while above should be satisfied as an image of the discrete Fourier transform. It also leads that the entries in the blue region should be zero, since those in the red region are zero from the algebraic range condition. Zero entries 0_{ab} in the blue region corresponds to same one in the red region. The discrete Fourier transform also requires $\alpha = -\zeta$ and $\beta = \epsilon$, etc.

Since $\{g^*_{n,k}\}$ is supposed to be an image of discrete Fourier transform (5.2), they should satisfy $g^*_{n,k} = \overline{g^*_{N-n,K-k}}$ for all n and k, which is indicated by the above line in Fig. 5. This is realized in the step (4a) and (4b). Note that the process (4b) is consistent to the algebraic range condition. For instance, in the step (4b) we modify $g^*_{-1,2}$, $g^*_{-3,2}$, $g^*_{-5,6}$, and $g^*_{-7,6}$ which keep to enjoy $g^*_{-1,2} = -\overline{g^*_{-3,2}}$ and $g^*_{-5,6} = -\overline{g^*_{-7,6}}$.

We present three numerical experiments with different type of noisy data. We generate the data for a function f modeled on a modified Shepp-Logan phantom in $E = \{(x_1/0.69)^2 + (x_2/0.92)^2 < 1\}$ inscribed in the unit disc Ω. Outside E we set $f \equiv 0$. In the reconstructions below we use the numerical algorithm in [2], based on the A-analytic theory [1]. This avoids the interpolation error that would occur due to the translation of the data from the torus to the tangent bundle of the circle, the latter being needed in a standard filtered back projection algorithm. For discretization we use $K = N = 256$.

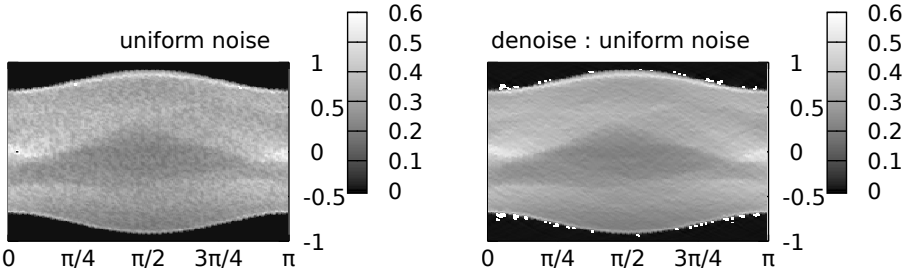

Fig. 6. Sinogram generated by specifying uniform random noise of 20% magnitude, which has 11.5% relative error in the L^2 sense (left) and denoised one by the projection to $AR(X)$ with 5.9% relative L^2 error (right)

In the first experiment the exact data Xf^{exact} is corrupted by some additive uniformly distributed noise δ of 20% magnitude, which is approximately 11.5% in the relative L^2 sense and is given in the left figure of Fig. 6 as sinogram. The reconstruction is performed from this noisy data $Xf^+ := Xf^{\text{exact}} + \delta$ in two different ways and shown in Fig. 7: On the left the reconstruction is obtained from the "raw" data Xf^+. This reconstruction (restricted to the elliptical region E) has a 53.1% relative error in the L^2 sense. The reconstruction in Fig. 7 on the right is obtained from inverting the projection of Xf^+ on the range $AR(X)$. This reconstruction has an error of 34.5% in the relative L^2-sense.

Next we show the results in the two extreme case scenarios: the worst case, when the entire noise lies in the algebraic range and in the best case, when the entire noise is orthogonal to the algebraic range.

In order to simulate some noise which lies entirely in the algebraic range $AR(X)$, or lies entirely in $AR(X)^\perp$, we use the knowledge of Xf^{exact} and decompose the existing noise δ into its component $\delta^{AR} \in AR(X)$, respectively $\delta^\perp \in AR(X)^\perp$ as follows.

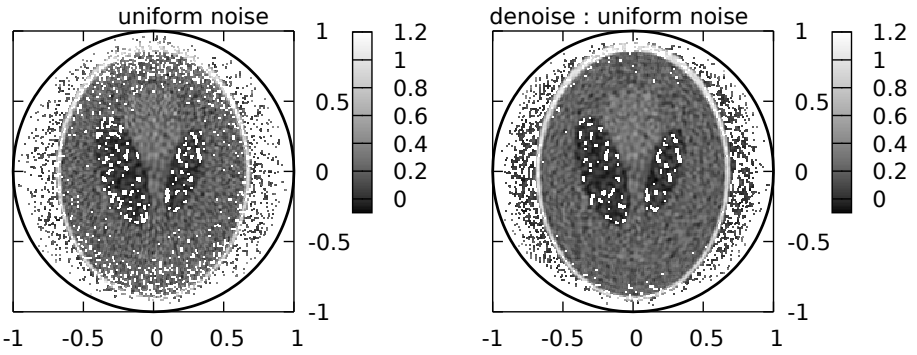

Fig. 7. Reconstruction results; (left) Reconstruction from noisy data Xf^+ in the left figure of Fig. 6, (right) Reconstruction from denoised data Xf^* by the projection onto $AR(X)$ depicted in the right one in Fig. 6. Xf^+ contains uniform random noise of 20% magnitude.

For $\delta := Xf^+ - Xf^{\text{exact}}$ compute its Fourier coefficients $\delta_{n,k}$ as in (5.2). Then find $\delta^{AR}_{n,k}$ by projecting $\delta_{n,k}$ on $AR(X)$ via Step 3 of the algorithm. The component δ^{AR} is found by Step 4 in the algorithm, and the discrete inverse Fourier transform of $\{\delta^{AR}_{n,k}\}$ via (5.3). We also set $\delta^{\perp} := \delta - \delta^{AR}$.

Fig. 8 on the left shows the data corrupted by some noise lying entirely in the algebraic range $Xf^{\text{exact}} + \delta^{AR}$, and Fig. 9 on the left displays the reconstructions from this data. The reconstruction in Fig. 9 on the right first performs a projection on $AR(X)$ and then performs the inversion from it. Both reconstructions (restricted to the ellipsoid E) in Fig 9 contain approximately 34.5% relative L^2 error, confirming that, in this worst case scenario, the projection method does not bring any improvement. Indeed, this was expected, since the noise in the data was artificially created to lie in $AR(X)$.

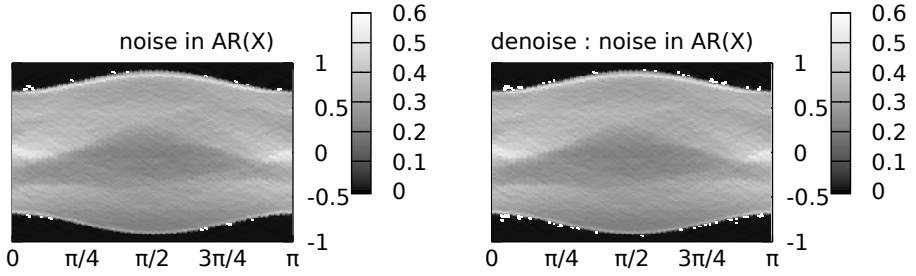

Fig. 8. Sinogram of $Xf^{\text{exact}} + \delta^{AR}$ with 5.8% relative L^2 error (left) and denoised one by the projection with 5.9% relative L^2 error (right)

The best case scenario is when the entire noise happens to be orthogonal to the algebraic range. Fig. 10 on the left depicts such noisy data $Xf^{\text{exact}} + \delta^{\perp}$, while Fig. 11

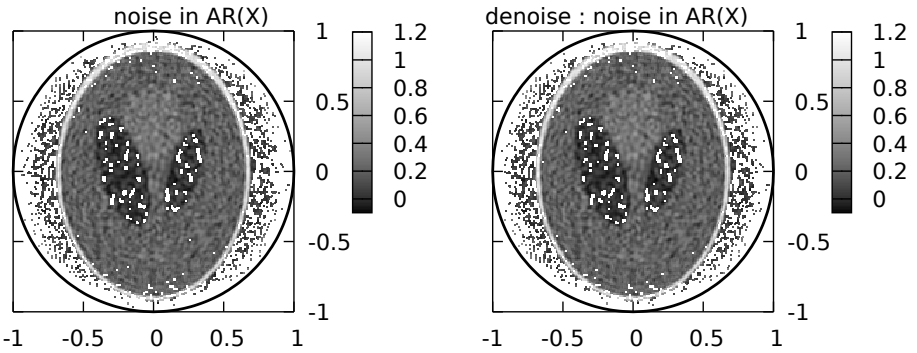

Fig. 9. Worst case scenario: The data $Xf^{\text{exact}} + \delta^{AR}$ has 5.8% relative L^2-error. Left: the reconstruction from this data has 34.5% error in E. Right: the reconstruction from denoised data also has 34.5% error in E. Since the noise was entirely in the algebraic range, the projection is redundant.

on the left depicts the reconstruction from this "raw" data. In contrast, Fig. 10 on the right shows the projection of the noisy data on the algebraic range, while Fig. 11 on the right shows the inversion from this projection.

Reconstruction from the noisy data in Fig. 11 on the left has 45.2% error in the relative L^2 sense, whereas the reconstruction in Fig. 11 on the right has a 19.4% relative L^2- error. In this best case scenario, one can observe that the reconstruction result shown in right figure is dramatically improved by our "denoising" algorithm. We also note that in this best case scenario example the raw data $Xf^{\text{exact}} + \delta^{\perp}$ had a larger error than $Xf^{\text{exact}} + \delta^{AR}$, but because it was orthogonal to the range, the reconstruction from its projection on $AR(X)$ gave an accurate reconstruction image; see Fig. 11 on the right.

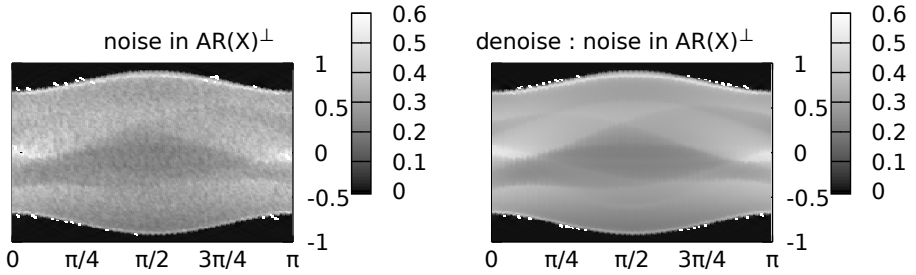

Fig. 10. Sinogram of $Xf^{\text{exact}} + \delta^{\perp}$ with 10.0% relative L^2 error (left) and denoised one by the projection with 1.2% relative L^2 error (right)

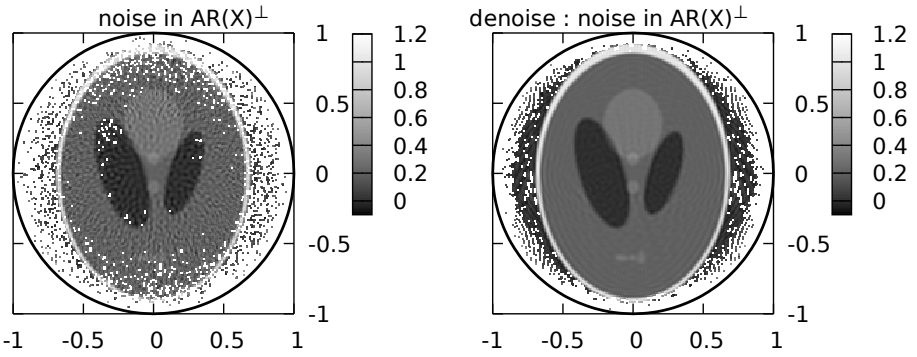

Fig. 11. Best case scenario: The data $Xf^{\text{exact}} + \delta^{\perp}$ has 10.0% relative L^2- error. Left: the reconstruction from this data has 45.2% relative L^2-error. Right: the reconstruction via the proposed denoising method has 19.4% relative L^2- error. Since the noise was entirely orthogonal to the algebraic range, the projection method is most effective.

Acknowledgement.

The work of H. Fujiwara was supported by JSPS KAKENHI Grant Numbers JP20H01821 and JP22K18674. The work of K. Sadiq was supported by the Austrian Science Fund (FWF), Project P31053-N32. The work of A. Tamasan was supported in part by the National Science Foundation DMS-1907097.

References

1. Bukhgeim, A.L.: Inversion formulas in inverse problems. In: Linear Operators and Ill-Posed Problems by Lavrentiev, M.M. and Savalev, L.Ya., pp. 323–378. Plenum, New York (1995)
2. Fujiwara, H., Tamasan, A.: Numerical realization of a new generation tomography algorithm based on the Cauchy-type integral formula. Adv. Math. Sci. Appl. **28**(2), 413–424 (2019)
3. Gel'fand, I.M., Graev, M.I.: Integrals over hyperplanes of basic and generalized functions. Soviet Math. Dokl. **1**, 1369–1372 (1960)
4. Gompel, G.V., Defrise, M., Dyck, D.V.: Elliptical extrapolation of truncated 2D CT projections using Helgason-Ludwig consistency conditions. In: M.J. Flynn, J. Hsieh (eds.) Medical Imaging 2006: Physics of Medical Imaging, vol. 6142, p. 61424B. International Society for Optics and Photonics, SPIE (2006). DOI 10.1117/12.653293
5. Helgason, S.: The Radon transform on Euclidean spaces, compact two-point homogeneous spaces and Grassmann manifolds. Acta Math. **113**, 153–180 (1965). DOI 10.1007/BF02391776
6. John, F.:The ultrahyperbolic differential equation with four independent variables. Duke Math. J., **4(2)**, 300–322 (1938).
7. Karp, J.S., Muehllehner, G., Lewitt, R.M.: Constrained fourier space method for compensation of missing data in emission computed tomography. IEEE Trans. Med. Imag. **7**(1), 21–25 (1988). DOI 10.1109/42.3925
8. Kudo, H., Saito, T.: Sinogram recovery with the method of convex projections for limited-data reconstruction in computed tomography. J. Opt. Soc. Am. A Opt. Image Sci. Vis. **8**(7), 1148–1160 (1991). DOI 10.1364/JOSAA.8.001148

9. Ludwig, D.: The Radon transform on euclidean space. Comm. Pure Appl. Math. **19**, 49–81 (1966). DOI 10.1002/cpa.3160190207
10. Monard, F.: Efficient tensor tomography in fan-beam coordinates. Inverse Probl. Imaging **10**(2), 433–459 (2016). DOI 10.3934/ipi.2016007
11. Nadirashvili, N.S., Sharafutdinov, V. A., Vlădut S.G.: The John equation for tensor tomography in three-dimensions. Inverse Problems **32(10)**: 105013, (2016).
12. Pantyukhina, E.Y.: Description of the image of a ray transformation in the two-dimensional case. In: Methods for solving inverse problems (Russian), pp. 80–89, 144. Akad. Nauk SSSR Sibirsk. Otdel., Inst. Mat., Novosibirsk (1990)
13. Patch, S.K.: Moment conditions indirectly improve image quality. In: Radon transforms and tomography (South Hadley, MA, 2000), *Contemp. Math.*, vol. 278, pp. 193–205. Amer. Math. Soc., Providence, RI (2001). DOI 10.1090/conm/278/04605
14. Pestov, L., Uhlmann, G.: On characterization of the range and inversion formulas for the geodesic X-ray transform. Int. Math. Res. Not. IMRN **2004**(80), 4331–4347 (2004). DOI 10.1155/S1073792804142116
15. Sadiq, K., Tamasan, A.: On the range of the attenuated Radon transform in strictly convex sets. Trans. Amer. Math. Soc. **367**(8), 5375–5398 (2015). DOI 10.1090/S0002-9947-2014-06307-1
16. Sadiq, K., Tamasan, A.: On the range of the planar X-ray transform on the fourier lattice of the torus (2022). arXiv:2201.10926, under review.
17. Sadiq, K., Tamasan, A.: On the range of the X-ray transform of symmetric tensors compactly supported in the plane. Inverse Probl. Imaging **17**(3), 660–685 (2023). DOI 10.3934/ipi.2022070
18. Sharafutdinov, V.A.: Integral geometry of tensor fields, *Inverse Ill-posed Probl. Ser.*, vol. 1. VSP, Utrecht (1994). DOI 10.1515/9783110900095
19. Xia, Y., Berger, M., Bauer, S., Hu, S., Aichert, A., Maier, A.: An improved extrapolation scheme for truncated CT data using 2D Fourier-based Helgason-Ludwig consistency conditions. Int. J. Biomed. Imaging pp. 1867025, 14 pages (2017). DOI 10.1155/2017/1867025
20. Yu, H., Wang, G.: Data consistency based rigid motion artifact reduction in fan-beam CT. IEEE Trans. Med. Imaging **26**(2), 249–260 (2007). DOI 10.1109/TMI.2006.889717
21. Yu, H., Wei, Y., Hsieh, J., Wang, G.: Data consistency based translational motion artifact reduction in fan-beam CT. IEEE Trans. Med. Imaging **25**(6), 792–803 (2006). DOI 10.1109/TMI.2006.875424